EFFECT OF NEUTRON IRRADIATION ON FRACTURE RESISTANCE OF ADVANCED SIC/SIC COMPOSITES—K. Ozawa, Y. Katoh, L.L. Snead (Oak Ridge National Laboratory), T. Nozawa (Japan Atomic Energy Agency)

OBJECTIVE

The objective of this work is to determine the neutron irradiation effects on fracture toughness of advanced nuclear grade SiC/SiC composites reinforced with advanced silicon carbide fibers.

SUMMARY

In order to identify the neutron irradiation effects on fracture resistance of advanced SiC/SiC composites, unloading-reloading single edge notched bend tests were conducted and an analytical model based on non-linear fracture mechanics was applied. As a result of the analysis, energy release rate contributed by macro-crack initiation of 3.1 kJ/m^2 for both unirradiated and irradiated advanced SiC/SiC composites (Hi-Nicalon Type-S (0°/90° plain woven) / multilayer / chemically vapor infiltration) is estimated. This result indicates no significant degradation in fracture resistance after neutron irradiation to 5.9×10^{25} n/m^2 at 800°C.

PROGRESS AND STATUS

Introduction

A silicon carbide fiber reinforced silicon carbide matrix (SiC/SiC) composite is an attractive candidate material for structural and functional components in fusion energy systems due to its good radiation stability coupled with inherently low induced radioactivity and after-heat [1, 2].

The focus on irradiation study of SiC/SiC composites in the past few decades has been mainly 'material screening,' but this phase is coming to a close. In recent years, multidirectional, statistical evaluation of mechanical properties using the "reference nuclear grade" SiC/SiC composites has been studied. Nuclear grade materials are generally defined as containing stoichiometric SiC fibers infiltrated with a matrix by chemically vapor infiltration (CVI), or the class of nano-infiltration and transient eutectic-phase (NITE) ceramics.

For the new class of nuclear grade composites, determining fracture resistance is one of the most important issues to be investigated. However, this is quite difficult because composites consist of several constituents and hence the fracture toughness of composites with non-uniform properties cannot be determined by simply applying a compliance method based on linear elastic fracture mechanics (LEFM). For example, Droillard *et al.* extended LEFM for composites using a two-step approach, in which the fracture behavior was subject to the combination of two parallel ideal composite systems [3]. In the current study, we try to apply non-linear fracture mechanics, based on actual crack increment measurements. While there has been a vigorous effort to study the irradiation effects in the SiC/SiC composite system [4-8], there are no published result on the effects of irradiation on fracture toughness. It is noted that an abstract on the subject, utilizing Hi-Nicalon™ Type-S fiber reinforced SiC matrix composites after neutron irradiation to 4.3×10^{24} n/m^2 at 40ºC, was located [9].

The main objective of this study is to determine the neutron irradiation effects on fracture toughness of advanced nuclear grade SiC/SiC composites. For this purpose, unloading-reloading tests and direct observations of crack propagation were conducted. Additionally a new analysis based on energy balance for composites' fracture resistance has been applied.

Experimental Procedure

Description of the material used is listed in Table 1. In this study, Tyranno™-SA3 or Hi-Nicalon™ Type-S

2D fabric-reinforced, chemically vapor infiltration (CVI) SiC matrix composites with 50 and 150 nm-thick pyrolytic carbon (PyC) or PyC/SiC multilayer interphase were prepared. The specimens were machined to miniature pre-notched rectangular beams for in-plane mode-I fracture toughness evaluation. Figure 1 is a drawing of the single edge notched bend (SENB) specimen. These miniature notched specimens were used because of the limitation of irradiation capsule volume. Three tests can be conducted with one specimen. The size effects on fracture resistance of advanced SiC/SiC composites are discussed elsewhere [10, 11], and notch insensitivity was demonstrated. Test coupons including an artificial notch were machined from the composite plate using a diamond saw. The radius of the notch root was approximately 150 μm. It is noted that the notch depth to width ratio was fixed for all specimens (a/W= 0.50). One side of the specimen surface was polished with 1 μm diamond film to aid in crack extension observation. Detailed information about the material fabrication and characterization before/after neutron irradiation is given elsewhere [12, 13].

Neutron irradiation was in the high flux isotope reactor (HFIR) at the Oak Ridge National Laboratory. The peak neutron fluence was ~5.9×10^{25} n/m^2 (E>0.1MeV), while the nominal irradiation temperature was ~800°C (HFIR-18J). An equivalence of one displacement per atom (dpa) = 1×10^{25} n/m^2 (E > 0.1 MeV) is assumed for these irradiations.

The SENB tests were conducted at room-temperature using an electromechanical testing machine (Insight 10, MTS Systems Co.) with a load capacity of 10 kN with ±0.26 % precision. Test specimens were loaded using a three-point bend fixture with a support span of 16 mm under a constant crosshead displacement rate of 0.05 mm/min. Crack opening displacement (COD) was measured by a clip-on gauge attached to a pair of aluminum tabs. The unloading-reloading sequences were applied to evaluate the damage accumulation behavior during testing. After each loading-unloading cycle, the test specimen was removed from the test machine in order to make replica images. Acetobutyrate (Tacphan) replicating sheets with a thickness of 100μm were used. Replicas at each damage level were observed by conventional optical microscopy.

Results and Discussion

Typical load-COD curves of advanced SiC/SiC composites before/after neutron irradiation are reproduced in Fig. 2. As shown in Fig. 2 (b), (c) and (d), the composites reinforced with Hi-Nicalon Type-S (A, E and M) exhibited typical quasi-ductility. In Fig. 2 (c) and (d), the change in crack length is also plotted from the microscopic measurements on the replica films. As an example, the optical micrographs of the replica images for the M7C specimen were shown in Fig. 3. According to this result, the fracture behavior consists of three stages as follows: [i] deformation induced not by macro-crack but micro-crack, [ii] linear increase of macro-crack, and [iii] crack branching and load transfer by friction at the fiber/matrix interface and fiber fracture (Fig. 2 (c) and (d)). In contrast to the Hi-Nicalon Type-S behavior, the composites reinforced with Tyranno-SA3 fiber (samples T, X and F) exhibited relatively low quasi-ductility. This is primarily attributed to very high interfacial strength caused by the thin interphase and large fiber roughness, which results in rapid crack extension. No significant change in the load-COD curves following neutron irradiation are observed for either composite type. This is in agreement with the result of tensile property evaluations [13].

The test results apparently show quasi-ductility of composites with F/M interphase, i.e., energy consumption during irreversible damage accumulation beyond matrix cracking. Therefore, considering separately the contributions from irreversible energies such as interfacial friction, thermal-residual strain energy, and fiber fracture becomes a key issue. Because of this quasi-ductility, using an analytical model based on non-linear fracture mechanics [14, 15] is reasonable. Hence, the analytical method developed by Nozawa *et al.* [10, 11] has been applied. In this model, the total work during the notched specimen test (w) is defined in Fig. 4 as:

$$w = U_e + U_{fr} + U_r + \Gamma_{total} \quad (1)$$

, where U_e is elastic energy, U_{fr} friction energy at the interface, U_r the residual strain energy, and Γ_{total} the crack surface formation energy. It is noted that the crack surface formation energy includes both micro- and macro-crack-forming energies. Then, the fracture resistance (G_{total}) can be written as:

$$G_{total} = \frac{\partial \Gamma_{total}}{t \partial a} = \frac{1}{t} \frac{\partial \Gamma_{total}}{\partial x} \frac{\partial x}{\partial a} \tag{2}$$

with a being the crack length, t the specimen thickness, and x the crack opening displacement.

Following the definition in Fig. 4, the crack surface formation energy of the M composite before/after irradiation was plotted as a function of crack opening displacement in Fig. 5. From Fig. 5, it is apparent that the crack surface formation energy rapidly increases with damage accumulation. Of particular note is that the crack surface formation energy seems proportional to the crack opening displacement in the stage [ii]. Combining the stage [ii] data of the crack length change in Fig. 2 (c), (d) and the crack surface formation energy change in Fig. 5, apparent fracture resistances of ~4.22 kJ/m^2 at macro crack initiation for the unirradiated composite and ~4.37 kJ/m^2 for the irradiated composite were obtained using Eq. (2).

However, as depicted above, the fracture resistance defined in Eq. (2) cannot unambiguously distinguish between contributions from micro- and macro-crack formation. In this study, a macro-crack is defined as the main crack that can lead to failure of a composite, and it is assumed that such main crack initiates at the peak load. Micro-cracks are the cracks that do not contribute to the main crack directly and are formed just after the proportional limit, such as the matrix cracks formed along the fiber longitudinal direction. Since the fracture resistance is determined by the main crack extension, it should be evaluated as the contribution of only macro-cracks, not including any contribution of micro-crack accumulation. Figure 4 also gives a schematic illustration for determination of the energy release rate during micro-crack formation from the load-displacement curve. From the figure, micro-crack surface formation energy was empirically obtained as:

$$\Gamma_{micro} \cong \sum_{i=1}^{n} C_i \left(1 - \frac{a}{W}\right)^i \tag{3}$$

, where Γ_{micro}, C_i (i=1,2, …, n), W are the micro-crack surface formation energy, constants, and specimen width, respectively. An energy release rate for micro-crack (G_{micro}) is then defined as follows:

$$G_{micro} \equiv -\frac{\Delta \Gamma_{micro}}{t \Delta a} \cong \frac{1}{Wt} \sum_{i=1}^{n} i C_i \left(1 - \frac{a}{W}\right)^{i-1} \tag{4}$$

Simply applying a linear fit in Eq. (4), we obtained an energy release rate of ~1.25 kJ/m^2 for unirradiated and ~1.11 kJ/m^2 for irradiated tests. Eventually, the actual fracture resistance for macro-crack (G_{macro}) is simply given by $G_{macro} = G_{total} - G_{micro}$. As a result, ~3.1 kJ/m^2 was estimated for both composites, before and after irradiation, indicating no significant degradation for the neutron irradiation conditions studied.

Acknowledgement

The authors would like to thank Ms. A.M. Williams, Mr. L.T. Gibson, Ms. P.S. Tedder, Ms. A.D. Harrison, Ms. S.G. Beck and Mr. L.E. Reid for post-irradiation experiments. Irradiation was carried out in the Department of Energy High Flux Isotope Reactor User Facility. This research was sponsored by the Office of Fusion Energy Sciences, US Department of Energy under contract DE-AC05-00OR22725 with UT-Battelle, LLC. This study was also a part of 'JUPITER-II (currently TITAN)' US Department of Energy/Japanese Ministry of Education, Culture, Sports, Science and Technology (MEXT) collaboration for

fusion material system research.

References

[1] T. Nozawa, T. Hinoki, A. Hasegawa, A. Kohyama, Y. Katoh, L.L. Snead, C.H. Henager Jr, J.B.J. Hegeman, J. Nucl. Mater. 386-388 (2009) 622.

[2] Y. Katoh, L.L. Snead, C.H. Henager Jr, A. Hasegawa, A. Kohyama, B. Riccardi, H. Hegeman, J. Nucl. Mater. 367-370 (2007) 659.

[3] C. Droillard, P. Voisard, C. Heibst, J. Lamon, J. Am. Ceram. Soc. 78 (1995) 1201.

[4] T. Nozawa, Y. Katoh, L.L. Snead, J. Nucl. Mater. 384 (2009) 195.

[5] T. Nozawa, K. Ozawa, S. Kondo, T. Hinoki, Y. Katoh, L.L. Snead, A. Kohyama, J. ASTM Int. 2 (2005) 12884.

[6] K. Ozawa, T. Hinoki, T. Nozawa, Y. Katoh, Y. Maki, S. Kondo, S. Ikeda, A. Kohyama, Mater. Trans. 47 (2006) 207.

[7] K. Ozawa, T. Nozawa, Y. Katoh, T. Hinoki, A. Kohyama, J. Nucl. Mater. 367-370 (2007) 713.

[8] Y. Katoh, T. Nozawa, L.L. Snead, T. Hinoki, J. Nucl. Mater. 367-370 (2007) 774.

[9] G. Vekinis, K. Mergia, G. Xanthopoulou, Abstracts of International Symposium on New Frontier of Advanced Si-Based Ceramics and Composites (2004) 25.

[10] T. Nozawa, T. Hinoki, A. Kohyama, H. Tanigawa, Preprints of the 22nd IAEA Fusion Energy Conference FT/P2 (2008) 17.

[11] T. Nozawa, H. Tanigawa, J.S. Park, A. Kohyama, Ceram. Eng. Sci. Proc. 30 [10] (2009) 65, doi: 10.1002/9780470584002.ch6.

[12] Y. Katoh, K. Ozawa, L.L. Snead, Y.B. Choi, T. Hinoki, A. Hasegawa, Fusion Mater. DOE/ER-0313/45 (2008) 21.

[13] Y. Katoh, T. Hinoki, K. Ozawa, Y.B. Choi, A. Hasegawa, L.L. Snead, in these proceedings (2009).

[14] V. Kostopoulos, Y.P. Markopoulos, Y.Z. Pappas, S.D. Peteves, J. Eur. Ceram. Soc. 18 (1998) 69.

[15] M. Sakai, K. Urashima, M. Inagaki, J. Am. Ceram. Soc. 66 (1983) 868.

Table 1: Materials used in this study.

Name	Initial ID	Density [g/cm^3]	Fiber	Architecture	Interphase	Matrix
TySA-CVI-Ref	T	2.60	Tyranno-SA3	2D P/W [0°/90°]	150nm PyC	CVI
TySA-CVI-TI	X	2.60	Tyranno-SA3	2D P/W [0°/90°]	50nm PyC	CVI
TySA-CVI-TF	F	1.60	Tyranno-SA3	2D P/W [0°/90°]	150nm PyC	CVI
HNLS-CVI-Ref	A	2.50	Hi-Nicalon Type-S	2D P/W [0°/90°]	150nm PyC	CVI
HNLS-CVI-TI	E	2.50	Hi-Nicalon Type S	2D P/W [0°/90°]	50nm PyC	CVI
HNLS-CVI-ML	M	2.50	Hi-Nicalon Type S	2D P/W [0°/90°]	ML	CVI

Note: P/W; plain-woven, UD; uni-directional, PyC; pyrolytic carbon, ML; multi-layered, CVI; chemically vapor infiltration.

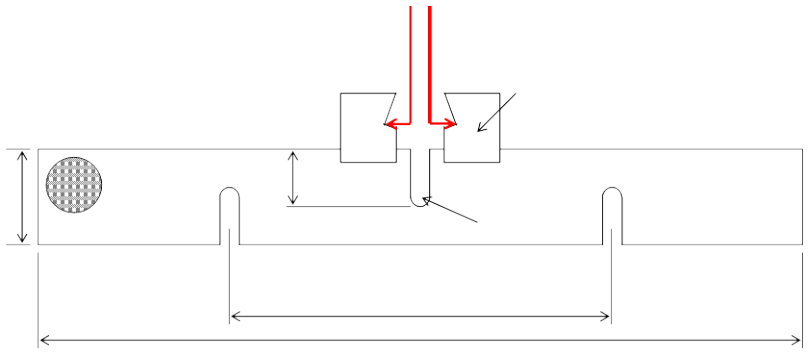

Fig. 1: Drawing of a miniaturized SENB specimen used in this study.

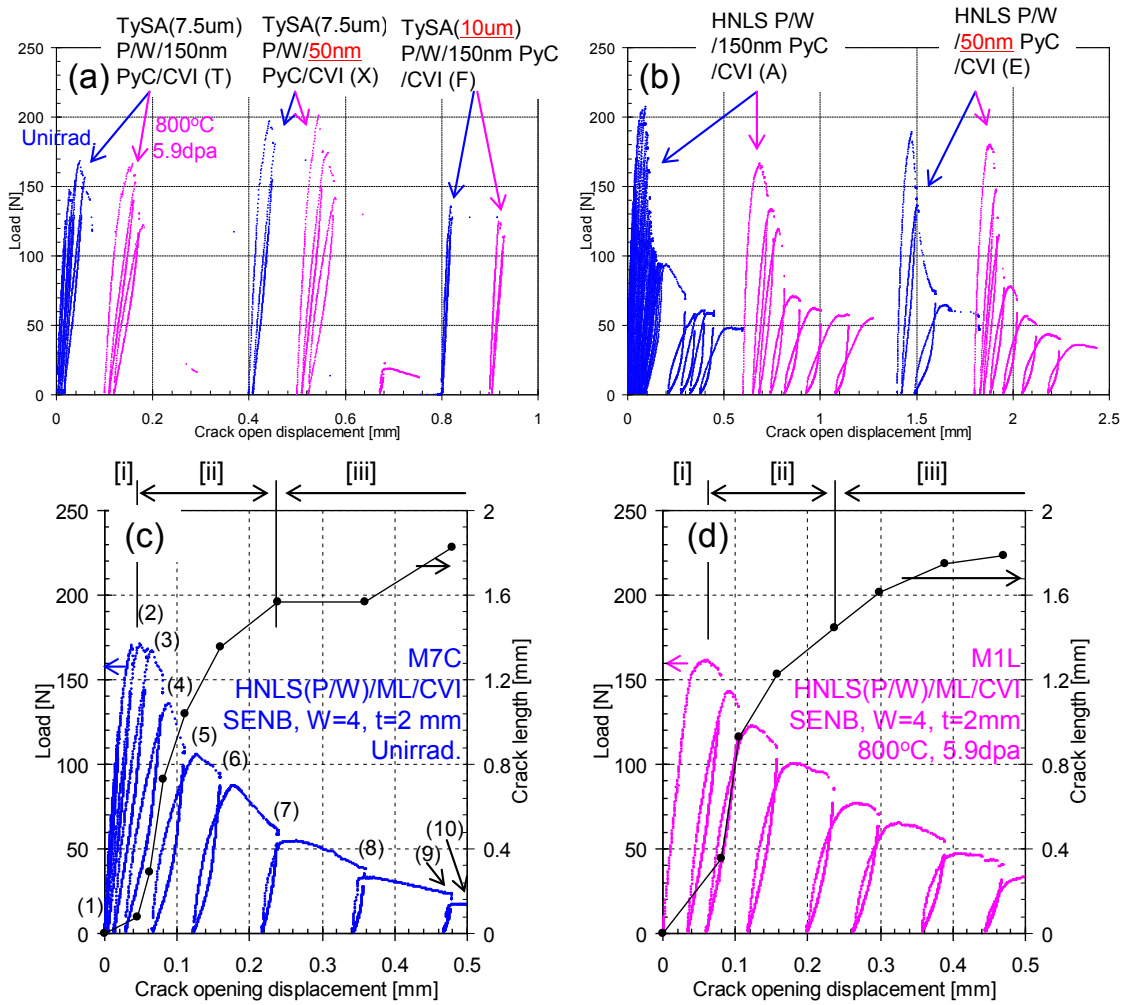

Fig. 2: Load-crack opening displacement curves. (a) TySA-CVI-Ref, -TI and -TF, (b) HNLS-CVI-Ref and -TI, (c) unirradiated HNLS-CVI-ML, and (d) irradiated HNLS-CVI-ML to 5.9dpa at 800°C.

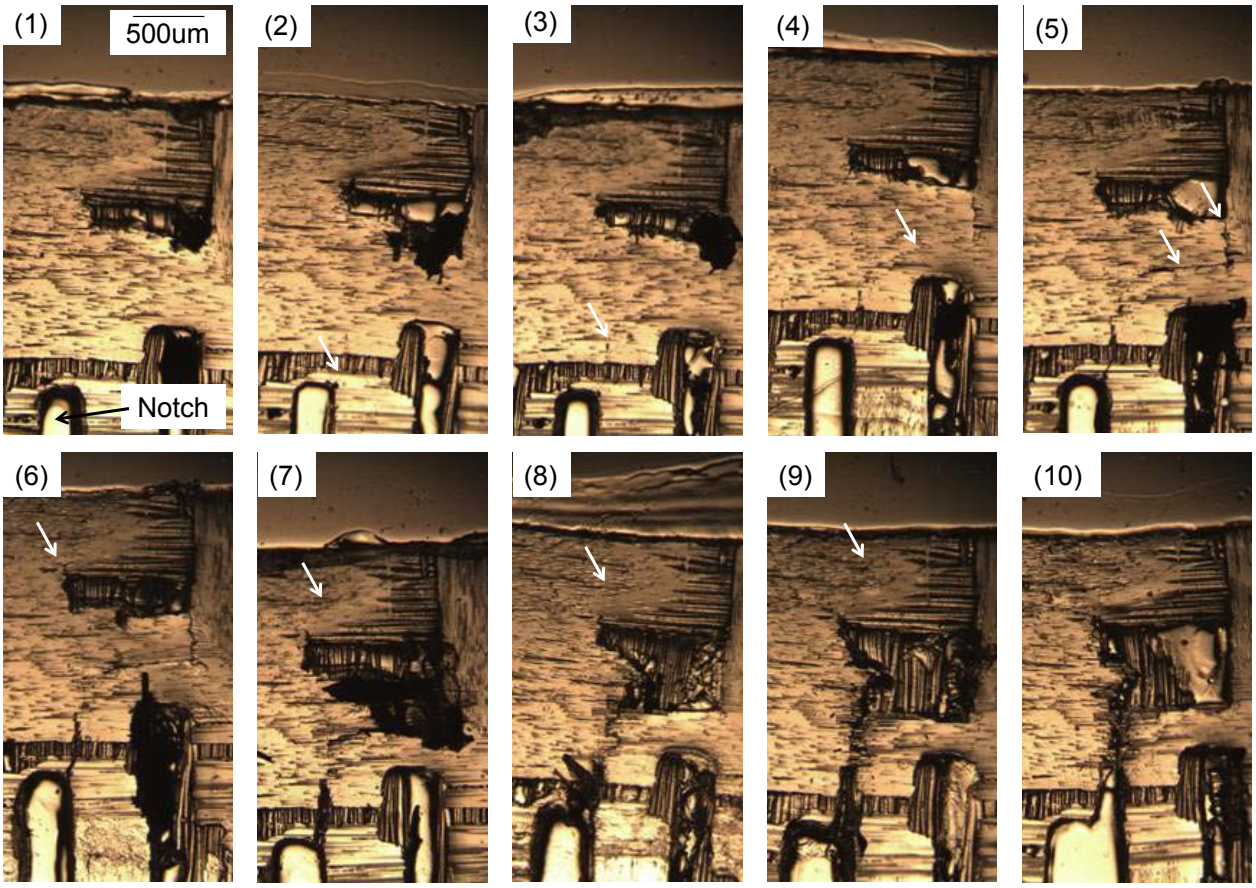

Fig. 3: Optical micrographs of crack in the unirradiated HNLS/ML/CVI composite (M7C). Arabic numbers in parenthesis correspond to each peak load in Fig. 2 (c).

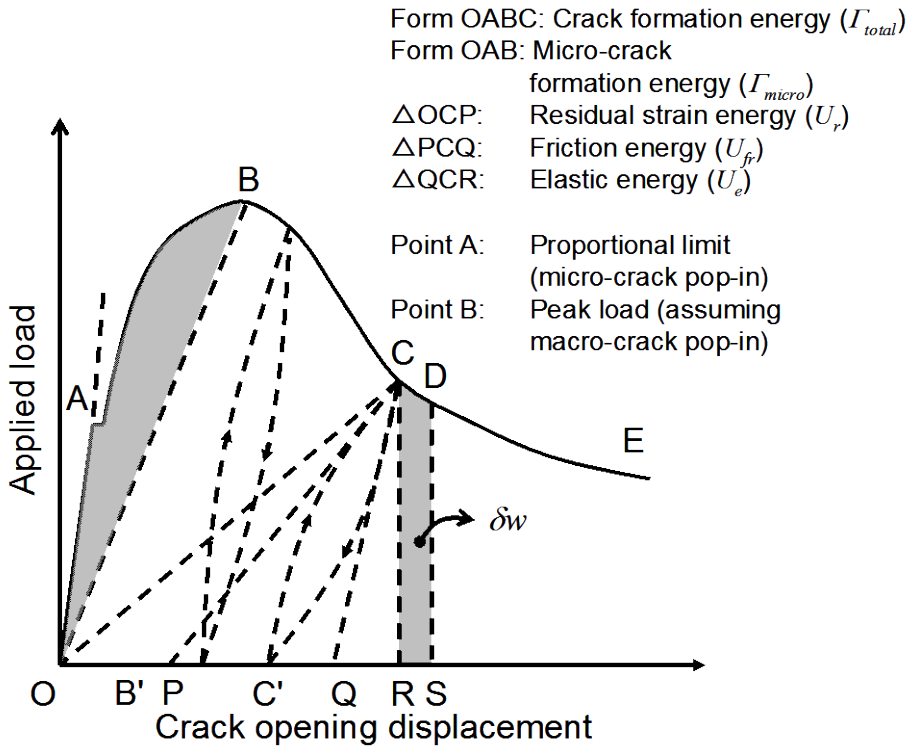

Fig. 4: Schematic illustration of load-crack opening displacement curve and definition of each energy.

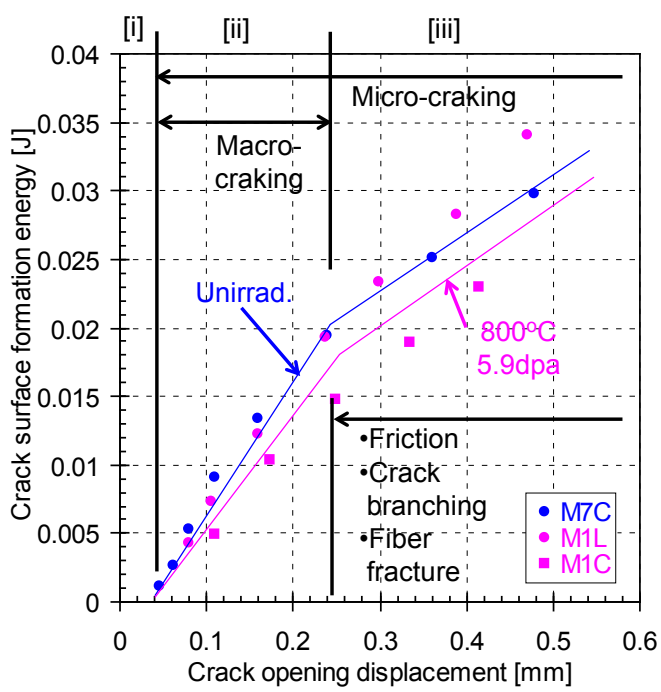

Fig. 5: Crack surface formation energy of unirradiated and irradiated HNLS (P/W)/ML/CVI (M).